JOURNAL OF MATERIALS SCIENCE 21 (1986) 825–836

Fabrication and characterization of rare earth hexaboride single-crystal materials

PAUL R. DAVIS, LYNWOOD W. SWANSON
Oregon Graduate Center, Beaverton, Oregon, USA
JOSEPH J. HUTTA
RADC/Solid State Sciences Division, Hanscom AFB, Massachusetts, USA
DOUGLAS L. JONES
Tektronix, Inc., Beaverton, Oregon, USA

Oriented single crystals of LaB_6, CeB_6 and PrB_6 have been prepared by the arc float-zone refining technique, which is described. A critique of the various possible preparation techniques is given. Wet chemical methods were used to determine bulk stoichiometries of samples prepared from starting materials of various R/B compositions (where R = rare earth). It was found that $LaB_{6.09}$, a desired composition, could be grown in single-crystal form from $LaB_{6.2}$ starting material, the excess boron compensating for preferential boron vaporization. Starting materials with B/La < 6.2 produce a B/La gradient in two-pass zone-refined specimens. The level of metallic impurities in arc zone-refined LaB_6 is lower than that reported elsewhere for laser zone-refined LaB_6. Residual oxygen present in the zone-refined specimens was found to produce second-phase inclusions, which were studied in detail. The effect of contamination of LaB_6 surfaces by evaporated refractory metals has also been investigated.

1. Introduction

The rare earth hexaborides (RB_6, where R = rare earth) exhibit an unusual combination of properties, having metallic conductivity and low work function as well as low volatility at temperatures providing technologically useful thermionic electron current densities. Thus, these materials are of interest for thermionic cathode applications.

The hexaboride LaB_6 has been studied most intensively, and has found practical use in a variety of microbeam applications. In this paper we present the results of work on the fabrication and characterization of single crystals of LaB_6, CeB_6 and PrB_6. Studies of volatility and work function of particular crystal planes of LaB_6 have been discussed elsewhere [1].

Earlier work on the rare earth hexaborides showed that precise bulk composition is an important parameter in determining the volatility and surface composition of these materials [2]. Surface composition, in turn, affects the work function of the face being examined and varies with temperature [1, 3]. In addition, the work function exhibits crystalline anisotropy, being higher on some crystal faces and lower on others. Because of these factors, great care must be exercised in the preparation of single-crystal specimens and in determining the crystal orientation and bulk stoichiometry of the samples studied.

2. Single-crystal preparation and mounting

The variety of methods which have been used successfully for growing rare earth hexaboride single crystals is summarized in Table I. Unlike many materials commonly prepared in large single-crystal form, the rare earth hexaborides have high melting points (e.g. 2715° C for LaB_6 [18]), posing the obvious problem of melt containment. For this reason, there has been no reported success in growing bulk single crystals of these materials by the Czochralski method of pulling from the melt, which is so useful in preparing single crystals of lower melting point materials.

The rare earth hexaborides are highly reactive at elevated temperature, and it is therefore necessary for crystal growth to be carried out in an inert atmosphere regardless of which technique is used. Furthermore, it is essential to maintain a considerable overpressure of inert gas where a large melt surface area is involved, in order to minimize material evaporation.

Growth of aligned aggregates of large single crystals by a modified Bridgman or directional solidification technique, using a cold crucible (skull melting) in the manner in which the stabilized cubic form of ZrO_2 is produced commercially [19], is a possibility which has not yet been explored. Success in this regard would open the door for development of larger area RB_6 cathodes. For many focused electron beam applications, thermionic cathodes of the order of a few millimetres in diameter are appropriate. This requirement can be met by the arc float-zone refining method [15], which can produce single-crystal rods of 1 to 3 mm diameter with outstanding reproducibility. An important advantage of this technique is the necessity for only minimal fabrication to finished cathode condition, compared with the coring or slabbing and

0022–2461/86 $03.00 + .12

TABLE I Summary of single-crystal growth methods

Method	Crystal size and shape	Orientation	Minimum impurity (p.p.m.)	Ref.
Molten aluminium flux	Needles (2 to 7 mm long) Plates (2 mm × 2 mm)	(1 1 0), (1 0 0)	1000*	[4, 5]
Electrolytic crystallization	Cubic (6 mm × 6 mm × 5 mm)	?	?	[6]
Float-zone with				
(a) r.f. heating	Rod (7 mm × 60 mm)	Random†	< 400	[7–9]
(b) laser heating	Rod (1.1 mm × 60 mm)	Selected	< 400	[10–12]
(c) electron beam heating	Rod (4 mm × 25 mm)	(1 0 0), (1 1 0), (1 1 1)	?	[13, 14]
(d) arc heating	Rod (3.0 mm × 30 mm)	Selected	45	[15]
Chemical vapour decomposition	Needles (2 to 5 mm long)	?	?	[16]
Vapour–liquid–solid (VLS)	Whiskers (1 to 4 μm diameter)	?	?	[17]

*Mostly clusters of aluminium-rich phase.
†Contained 1 mm^3 subgrain regions.

extensive grinding that would be necessary with bulk single-crystal boules.

Float-zone growth of single crystals of LaB_6 and other highly refractory compounds has been reported in which the molten zone was produced by CO_2 laser [10–12], electron beam [13, 14] and r.f. induction [7–9] heating. Despite the more complicated apparatus required for laser and electron beam float-zoning, the diameter of LaB_6 single-crystal rods produced is not significantly larger (3 to 4 mm) than those obtained using the simpler and less costly arc float-zoning apparatus. In addition, the absorptionof 10.6 μm CO_2 laser radiation is low for LaB_6, making it necessary to surround the molten zone with a spherical heat shield. Evaporation of material on to the heat shield and components of the focusing optics requires that the input power be varied continually when using the laser float-zone technique [11].

In the case of r.f. float-zone growth, crystal rod diameters of the order of 7 mm have been reported [7]. However, these rods do not appear to be truly single-crystal but consist of subgrains whose linear dimensions are about 1 mm, with angular misorientations ranging from several seconds to a few degrees. The r.f. or eddy-current heating approach used by Windsor [9] resulted in ingots 4 to 5 mm in diameter and 10 to 12 mm long. Again, these were not monocrystals but consisted of several large grains. By diamond sawing, it was possible to cut small bars 200 μm square in section for cathode fabrication.

Of all the techniques, float-zone melting has been developed most extensively. It is ideally suited to the growth of long, high purity crystals which may either be oriented as desired with a seed crystal during the zone pass, or cut into samples of the desired orientations. Seeded growth allows an arbitary axial orientation to be achieved, and is thus the more flexible technique for producing long crystals suitable for field and thermionic emission cathodes. To date, (1 0 0), (1 1 0), (1 1 1), (2 1 0), (2 1 1), (3 1 0), (3 4 6) and (3 2 1) oriented crystals of RB_6 compounds have been grown by the float zone seeding technique.

The zone-melting or float-zone method of preparing RB_6 crystals requires that a zone of the starting material, usually in the form of a hot-pressed (sintered) rod, be melted in a pressure ($\geqslant$ 1 atm) of inert gas, to reduce vaporization. The molten zone is then swept down the rod, carrying soluble impurities with it. Solidification behind the zone causes single-crystal growth and, if a single-crystal seed is used at the initiation of the zone, the solidified region will have the axial orientation of the seed. Usually two or three passes are required to achieve maximum purity of the sample.

We chose the arc float-zone melting technique from among the several float-zone methods. The melting was done in argon. By arc melting in argon, Verhoeven *et al.* [15] were able to produce high-quality LaB_6 crystals of 1 mm diameter and 2 to 3 cm length on a routine basis, using sufficiently pure (low-carbon) starting materials. From the standpoint of simplicity, low cost and achieving high purity and oriented single-crystal rods from which both flat and pointed emitter shapes can be fabricated, the arc float-zone method is preferable to other float-zone techniques.

In previous LaB_6 arc float-zone work, a tantalum counter electrode was used to establish and maintain the float-zone arc [15]. We have found that tantalum is unsuitable for PrB_6 refining, but that tungsten performs satisfactorily. However, the best counter electrode is a pointed piece of the starting material; that is, a pointed, hot-pressed rod of PrB_6 is the best counter electrode for PrB_6 zone refining. This statement also holds for LaB_6 and CeB_6. The improvement resulting from this modification is a more stable and controllable arc and the removal of potential electrode contaminants. A zone pass rate of 5 cm h^{-1} was used for preparing all RB_6 specimens in this study in order to prevent the well-known phenomenon of second-phase precipitation which occurs with more rapid cooling rates.

We have prepared seeded single-crystal rods of LaB_6, CeB_6 and PrB_6 by this method. Laue X-ray backscattering analysis of seeded ⟨1 0 0⟩ oriented rods shows that routine orientation to within 2° of the desired orientation is possible for all three compounds. Higher-index directions such as ⟨2 1 1⟩ and ⟨3 1 0⟩ have also been aligned along the rod axis to within 2°.

70° and 90° full cone angle emitters suitable for thermionic emission applications have been constructed by the use of mechanical grinding techniques. Typically RB_6 compounds can be conveniently

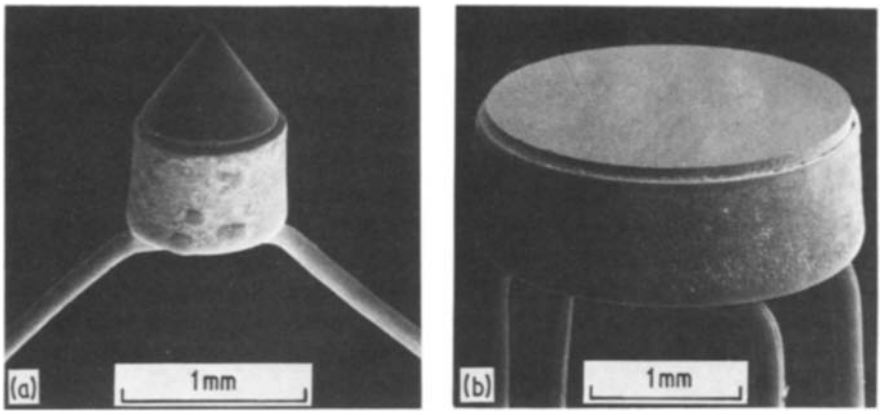

Figure 1 Typical mounting arrangement for RB_6 cathodes, brazed into rhenium cups: (a) pointed cathode for microbeam applications, (b) flat cathode for broad area applications.

ground using a 3000 mesh diamond wheel. For a smooth surface finish, a final polish using a 14 000 mesh aluminium oxide–diamond material is employed. The grinding step is very rapid, taking 3 to 4 min to fabricate a pointed end on an initially flat single-crystal rod of 1 mm diameter. If a truncated cathode is required, that step is performed next using the 3000 mesh diamond wheel.

Fig. 1 shows typical RB_6 cathode structures. In the overall mounting configuration the RB_6 crystal is brazed into a rhenium cup with a TaC braze, the cup in turn being mounted on resistively heatable tungsten filament supports. Cathodes mounted in this type of structure have operated successfully at 1800 K for over 1000 h. The heating characteristic curve for a 0.77 mm diameter flat cathode mounted in this fashion is shown in Fig. 2. One can achieve an operating temperature of 1800 K with ~ 2.5 W of electrical power for this structure.

A second type of mounting system used successfully for thermionic cathodes is the Vogel mount [20]. In this type of mount, the cathode is clamped between pyrolytic graphite blocks which are in turn held between heavy molybdenum or tungsten supports. The pyrolytic graphite has a higher resistance than the supports or the cathode. Thus, current passed through the assembly causes ohmic heating of the graphite, which heats the cathode by thermal conduction. The heavy supports are good heat sinks and never become hot enough to lose any material through vaporization, so there is no possibility of foreign material evaporating on to the cathode surface. This design is particularly suited to long lifetime applications, as will be discussed later.

3. Determination of sample stoichiometry

The rare earth hexaborides are compounds which exist over a range of stoichiometries. The bulk stoichiometry of the material has a strong effect upon the rate of vaporization at elevated temperature, and a less pronounced effect upon the work function. We therefore devoted considerable effort to the determination of sample stoichiometries.

Zone-refined RB_6 rods were analysed by wet chemical methods to determine precise stoichiometries. The most widely recommended technique [21] for precise assay of boron is the mannitol–borate

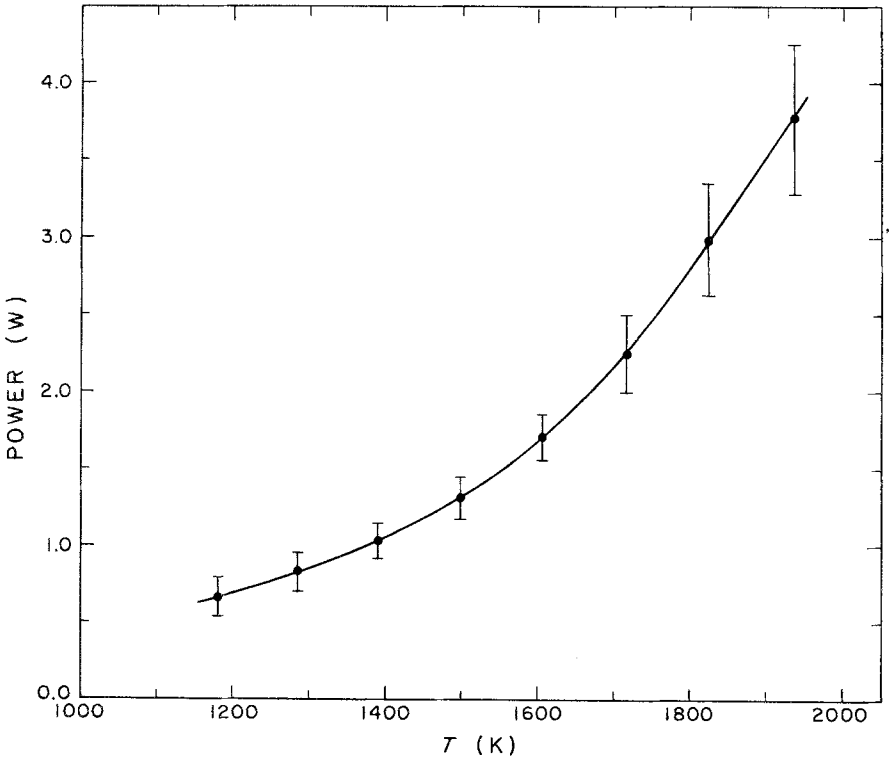

Figure 2 Heating power against temperature for LaB_6 cathode mounted as shown in Fig. 1a.

titration procedure in which excess acid used for dissolution of RB_6 is neutralized to pH 7, followed by addition of mannitol. This converts H_3BO_3 to a strong acid which can then be titrated with a strong base such as NaOH with an indicator or, as was the case in this work, with a pH meter in order to detect the end point. Prior to titration the R^{3+} was masked as a possible interfering ion by the addition of a slight excess of disodium ethylene diamine tetraacetate (EDTA) [22].

The rare earth metals were determined by a potentiometric titration against EDTA [23]. The reference electrode was either Ag–AgCl or $Hg–Hg_2Cl_2$, while the other electrode was a mercury-amalgamated gold wire. A few drops of $Hg^{2+}(EDTA)^{2-}$ were added to the sample solution in order to monitor the concentration of rare earth during the titration. Titration curves similar to those obtained during acid–base titrations are obtained by this technique, with the end-point occurring at the inflection point of the titration curve.

The detailed analytical procedure used was as follows. The RB_6 sample was dissolved in 1 : 1 HNO_3 at the rate of 6 ml dilute HNO_3 per 100 mg of RB_6. Up to about 200 mg of the hexaboride can be accommodated in a Parr acid digestion bomb which was heated for 10 min at $\sim 108°$ C. The resultant acidified solution of R^{3+} and H_3BO_3 was diluted with 50 ml of distilled water, neutralized to pH ~ 3 to 4 and diluted in a volumetric flask to $\sim 1\,g\,l^{-1}$ RB_6.

Powdered samples of LaB_6 from Cerac (Milwaukee, Wisconsin), quoted as being 99.9% pure, were too active for use of the Parr bomb. However, we recommend that the Parr bomb dissolution procedure be used for all RB_6 zone-refined samples, since this procedure greatly speeds up dissolution of RB_6 and also prevents loss of boron by volatilization of H_3BO_3, which has a significant vapour pressure at temperatures near 100° C.

A 25 ml pipetted aliquot of this solution was treated with an excess of EDTA, to which 25 ml of distilled water was added, and then neutralized to pH 7 with 20% KOH and 0.02 M KOH. After the addition of 6 to 8 g mannitol (1 g per 10 ml of solution) the titration was carried out using a pH meter to identify the end point.

The rare earth was determined by taking a 25 ml aliquot of the RB_6 solution, adding 25 ml of distilled water and neutralizing to pH $\sim$ 7. Next, 20 ml of 0.1 M acetic acid–sodium acetate buffer was added together with 6 drops of $Hg^{2+}(EDTA)^{2-}$ complex prepared by adding an equivalent amount of EDTA to 25 ml of 0.01 M $Hg(NO_3)_2$ solution. The titration was carried out potentiometrically using an Ag–AgCl reference electrode and an amalgamated gold wire which was periodically cleaned by immersion in dilute nitric acid. Typically 100 to 200 mV changes in potential occurred during a run, with steep drops in potential occurring at the end point.

Various other metal ions, e.g. Al^{3+} and Fe^{3+}, will interfere with lanthanum determinations and must be masked. Aluminium for example [24, 25] may be masked by the addition of sulphosalicyclic acid, and Fe^{3+} may be removed by reducing it with ascorbic acid.

4. Results of stoichiometry measurements

The technique of zone refining depends on the general thermodynamic principle of component fractionation between a liquid and the solid precipitating from that liquid during cooling. During cooling, the solid will tend to reject those components present in the liquid which lower the melting point of the solid. Such components include various impurities and excess major elements in compound or alloy starting materials [26].

The phase diagram of LaB_6, for example, shows a congruent melting composition of B/La $\approx$ 6.2, according to Storms and Mueller [2] (see Fig. 3a). Therefore, for a starting material with B/La < 6.2 one would expect the initial solid formed by a single zone pass to contain more boron than the feedstock, with the composition approaching that of the feedstock as the zone moves down the rod (Fig. 3b).

There is evidence, however, that for the B–La system, preferential vaporization of boron occurs from the liquid for compositions in the neighbourhood of B/La = 6. The liquid–vapour phase transition of this system has not yet been studied in detail, so the extent of preferential boron vaporization is not known. Furthermore, boron reaction with impurities such as carbon and oxygen in the molten zone may produce volatile boron-containing species which will also evaporate. Since this mechanism also removes the impurity, it would occur most significantly during the first zone pass, since the impurity concentration is dramatically reduced during the first pass.

The effect of preferential boron vaporization is to shift the sample composition toward the lanthanum-rich end of the phase diagram. The solid–liquid fractionation process has the opposite effect, at least at the start of the zone refining pass, if B/La < 6.2. Therefore, with starting material B/La < 6.2 one would expect the combination of mechanisms to produce a zone-refined LaB_6 specimen with reduced total boron content relative to the starting material, but with a concentration gradient such that B/La is higher at the beginning than at the end of the zone pass. Fig. 3a suggests that this effect would be more severe with B/La = 6.0 starting material than with B/La = 6.1, for example, because of the greater separation between liquidus and solidus curves at B/La = 6.0 and consequent greater solid–liquid fractionation.

We have investigated the effect of initial feedstock composition and number of zone passes on the stoichiometry of zone-refined LaB_6. When starting material of composition B/La = 6.0 is used, three or more zone passes will result in a reduced B/La ratio, a composition gradient and an observable lanthanum-rich second phase at the end of the zone pass, as predicted by the above discussion. These problems can be overcome by the use of starting material with B/La = 6.2 and the use of fewer zone passes. This technique has been successful in reducing the macroscopic appearance of second-phase material, and in driving the stoichiometry of the final material toward the optimum composition of 6.09. This composition seems to produce the maximum ratio of

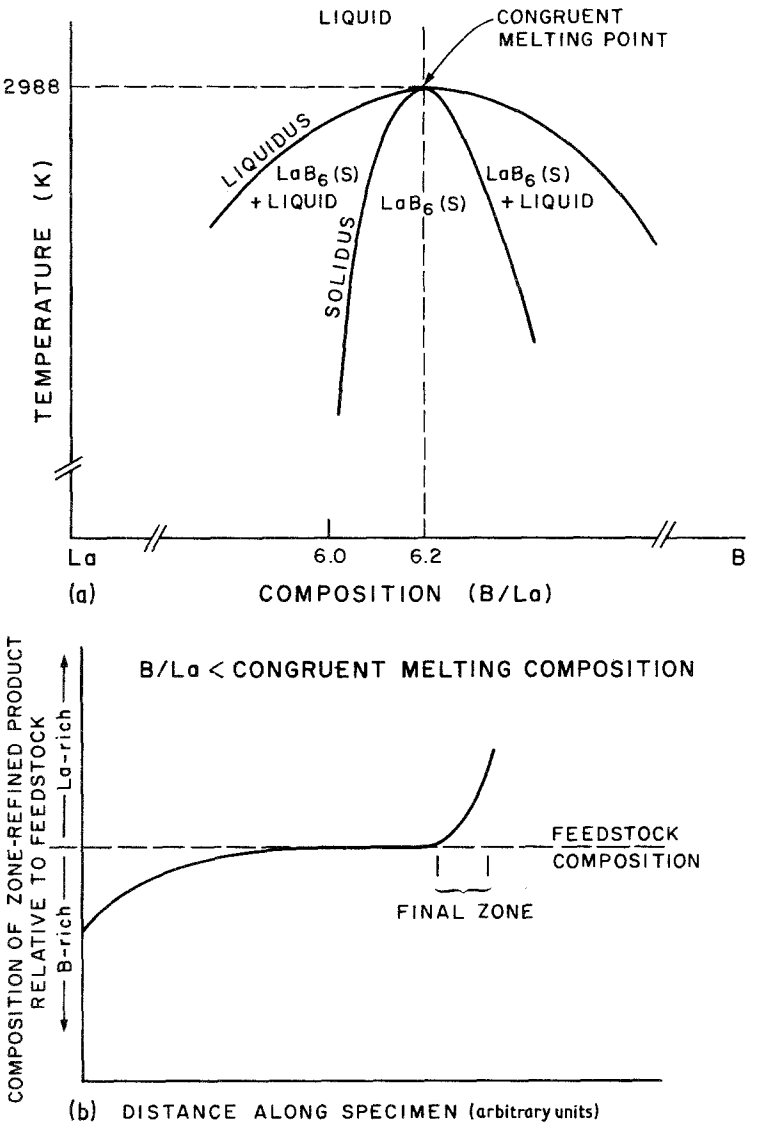

Figure 3 (a) Schematic representation of the La–B phase diagram in the region around the congruent melting point (adapted from data of Storms and Mueller [2]). (b) General form of composition profile of a zone-refined LaB_x specimen ($x < 6.2$) expected in the absence of preferential vaporization of boron.

emitted electron current to material vaporization for LaB_6.

Stoichiometry values determined for the zone-refined RB_6 rods prepared in this study are shown in Table II. Since the amount of material required for each analysis is relatively large, the uncertainty quoted in Table II reflects the estimated cumulative error in the analysis procedure. Actual stoichiometry variation from one zone-refining run to another has not been determined.

Note that results for the LaB_6 zone-refined specimens are qualitatively as predicted. The phase diagrams of CeB_6 and PrB_6 have not been as well characterized as that of LaB_6, so the zone-refined stoichiometry is impossible to predict. The fact that the CeB_6 zone-refined sample has a higher proportion of boron than the starting material might indicate that less boron evaporation (or more cerium evaporation) occurs than for LaB_6, or that the congruent melting point corresponds to $B/Ce < 6.0$. On the other hand,

TABLE II RB_6 composition before and after two zone passes

Feedstock (sintered)	Average	Beginning of pass§	End of pass¶	Starting material (p.p.m. by weight)		Two-pass zone-refined material (p.p.m. by weight)	
				Carbon	Oxygen	Carbon	Oxygen
$LaB_{6.1}$*	–	$LaB_{5.90\pm0.05}$	–	–	–	–	–
$LaB_{6.1}$*	$LaB_{5.8\pm0.1}$	$LaB_{5.94\pm0.05}$	$LaB_{5.71\pm0.05}$	–	–	–	–
$LaB_{6.2}$†	$LaB_{6.09\pm0.05}$	–	–	2160	13 100	40	240
$LaB_{6.2}$*	$LaB_{5.99\pm0.07}$	$LaB_{5.96\pm0.05}$	$LaB_{6.02\pm0.05}$	1700	790	60	10
$CeB_{6.0}$‡	$CeB_{6.2\pm0.1}$	–	–	950	7900	–	–
$PrB_{6.0}$‡	$PrB_{5.87\pm0.05}$	–	–	1410	28 800	–	–

*Demetron material (Demetron, Inc., Morgan Hill, California).
†MRC material (Materials Research Corp., Orangeburg, New York).
‡Cerac material (Cerac, Inc., Milwaukee, Wisconsin).
§First half of zone-refined rod, excluding end.
¶Last half of zone-refined rod, excluding final zone cooling region.

the PrB_6 behaviour is the same as expected for LaB_6. No attempt was made to produce zone-refined specimens with different B/Ce or B/Pr compositions.

5. Impurities in zone-refined LaB_6

5.1. Metallic impurities

Analysis of as-received and one-pass and two-pass zone-refined LaB_6 for impurities (other than carbon and oxygen) was done by an outside laboratory, using a spark mass-spectrometric technique. Table III shows the results of these analyses. The one-pass and two-pass results are for two different lots of starting material supplied by the same manufacturer, both with approximately the same initial impurity concentration (as listed). Only impurities with concentrations greater than 30 p.p.m. by weight in the starting material are listed in Table III.

The purification results shown in Table III are considerably better than equivalent results reported for laser zone-refined specimens. Table IV compares selected impurity level reductions observed here with values reported by others using both arc and laser float-zone techniques. The results reported by Takagi and Ishii [10] showed impurity levels at or near the detectability limits of the emission spectrography analysis techniques which they used, so their results represent conservative estimates of the efficacy of the laser zone-refinement technique. The data of Hohn *et al.* [11], however, seem to suggest that laser zone-refinement is relatively ineffective in removing impurities from LaB_6, and actually increases the concentrations of certain impurities. These authors had no explanation for this curious result, nor do we. In any case, it seems clear that arc float-zone refining is at least as effective as laser zone-refining in removing metallic impurities from LaB_6, and may possibly be more effective.

TABLE III Major impurities* in $LaB_{6.2}$ material obtained from MRC

Element	Content (p.p.m. by weight)		
	As-received	One-pass zone-refined	Two-pass zone-refined
W	240	5.2	< 0.14
Hf	75	< 0.15	< 0.15
Ba	59	< 0.27	< 0.27
Te	420	< 0.15	< 0.46
Sb	$> 10^4$	< 0.1	< 0.49
Sn	110	0.19	< 0.11
In	1100	< 0.1	0.10
Sr	200	< 0.1	< 0.1
As	86	< 0.1	0.10
Ge	46	0.14	0.14
Ga	41	0.88	< 0.1
Cu	85	0.16	0.18
Ni	190	3.1	2.6
Co	680	3.4	0.68
Fe	1300	21	0.70
Mn	130	< 0.63	0.19
Cr	1300	0.35	0.71
Ti	200	7.6	0.32
Ca	330	0.24	0.14
K	230	0.20	< 0.1
Cl	53	53	19
S	180	14	7.9
P	150	0.71	0.36
Si	$> 10^4$	3.0	7.1
Al	> 1900	< 9.3	3.1
Mg	2800	0.28	0.26
Na	79	< 53	< 0.1
Total	$> 3.2 \times 10^4$	< 225	< 100

*Values > 30 p.p.m.; carbon and oxygen not reported (see Table II).

5.2. Carbon and oxygen impurities

The LaB_6 samples were also analysed for carbon and oxygen. The results of these analyses are given in Table II. There is a dramatic variation in the concentrations of these impurities among starting materials from different producers, and between CeB_6 and PrB_6 from the same producer.

In previous studies of LaB_6 arc zone-refined material, Noack and Verhoeven [27] showed that the oxygen concentration was reduced in the first zone pass but not in subsequent zone passes. In that work, oxygen concentrations as low as 370 p.p.m. by weight in the starting material (obtained from Cerac) and 15 to 20 p.p.m. in the zone-refined material were observed. Because the oxygen concentrations measured in the zone-refined samples were so low, they were attributed to surface oxygen. Some of the samples we have studied exhibit much higher oxygen concentrations, which clearly cannot be attributed to surface adsorption alone. We believe that this oxygen is combined in a ternary second-phase material in the bulk. Zone-refined samples with ~ 10 p.p.m. oxygen have only recently been produced in our laboratory. The following discussion of defects applies to the zone-refined MRC starting material (Table II). The recently produced low oxygen-content specimens exhibit reduced defect concentrations, although they have not yet been studied in detail.

The carbon content of specimens we have analysed (Table II) is of the order of 50 p.p.m. after two zone passes. This result is in excellent agreement with an earlier study of carbon impurities in zone-refined LaB_6 performed by Noack and Verhoeven [27].

6. Defects in LaB_6 crystals

6.1. Bulk defects observed at cleaved surfaces

In order to study the perfection of LaB_6 single crystals, workers in the past have etched cleaved surfaces in HNO_3 solutions to preferentially enlarge defect pits and allow studies to be made by optical microscopy [10]. In this study a scanning electron microscope (SEM) was used to examine cleaved (1 0 0) LaB_6 surfaces. Because an SEM can resolve submicrometre features with ease, we found it unnecessary to etch or otherwise disturb the freshly cleaved surface.

Two distinctly different types of surface feature were observed in our SEM studies of cleaved (1 0 0) LaB_6. Type I features are square pits which average about 0.2 μm on a side and have sharp, square corners. Occasionally, two or three pits run together to form a rectangular feature. The average surface density of these pits for a single-pass rod was $\sim 2.5 \times 10^7$ cm^{-2}. In two-pass rods the pit density was $< 10^6$ cm^{-2}. In previous work using the HNO_3 etching technique,

TABLE IV Impurity levels and refinement efficiencies for selected metals in LaB_6: comparison of results

	Arc zone refinement										Laser zone refinement									
	This study*					Verhoeven *et al.* [15]†					Hohn *et al.* [11]‡					Takagi and Ishii [10]†				
	Al	Si	Ca	Fe	Mo	Al	Si	Ca	Fe	Mo	Al	Si	Ca	Fe	Mo	Al	Si	Ca	Fe	Mo
Starting material (p.p.m. by weight)	> 1900	> 10^4	330	1300	9.2	36 (2160)§	182 (259)	3005 (1639)	1625 (8029)	98 (2000)	80	80	230	1720	240	> 1000	50 to 100	> 1000	500 to 1000	–
Percentage of initial impurity remaining after one pass	< 0.4%	< 0.03%	0.07%	1.6%	7.5%	5% (< 0.01%)	< 0.2% (2.6%)	< 0.2% (< 0.08%)	1.8% (2.9%)	< 4.6% (18.5%)	112%	112%	8.7%	7.0%	75%	< 5 to 10%	~ 100%	< 1 to 5%	1 to 5%	–
Percentage of initial impurity remaining after two passes	< 0.2%	< 0.07%	0.04%	0.05%	1.4%	– (< 0.01%)¶	– (< 0.6%)¶	– (< 0.01%)¶	– (0.9%)¶	– (< 0.09%)¶	–	–	–	–	–	< 1%	~ 100%	< 1 to 5%	1 to 5%	–

*MRC material.
†Cerac material.
‡Haselden material. The authors quote impurity content (p.p.m.). We assume this to mean p.p.m. by weight.
§Quantities in parentheses refer to a second lot of starting material.
¶After three zone passes.

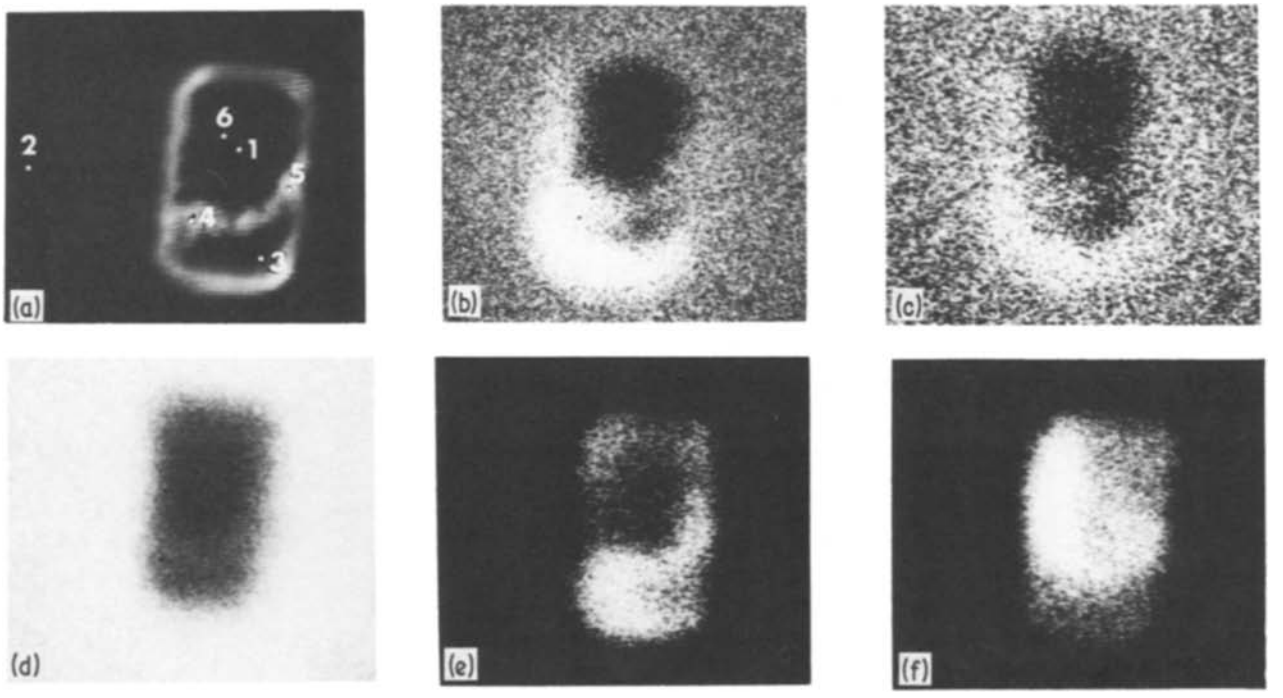

Figure 4 Scanning Auger maps of inclusion in (1 0 0) LaB_6 cleaved surface. (a) SEM photo; (b) La(NOO) map; (c) La(MNN); (d) B(KLL); (e) O(KLL); (f) C(KLL).

defect densities of $\sim 10^3\,cm^{-2}$ for aluminium flux-grown (1 0 0) LaB_6 [4] and $1.6 \times 10^6\,cm^{-2}$ for laser zone-refined (1 0 0) LaB_6 [10] cleaved surfaces have been measured. Hohn *et al.* [11] have reported etch pit densities of 5×10^5 to $10^7\,cm^{-2}$ for laser zone-refined LaB_6. The values reported here are thus of the same order of magnitude as those observed for the laser zone-refined material, but about three orders of magnitude larger than those for aluminium flux-grown crystals. The large concentration of these defects thus appears to be inherent in the zone-refinement process, but may depend somewhat upon the presence of impurities as suggested by the decrease in defect concentration which we have observed on the zone-refining second pass.

Type II surface features have linear dimensions approximately ten to twenty times larger than those of Type I, and are more sparsely distributed over the cleaved surface ($\sim 1 \times 10^4\,cm^{-2}$ in $LaB_{6.09}$ and $CeB_{6.2}$). They are more difficult to count because their density is extremely low. Each feature of this type is a square or rectangular pit with well-rounded corners, containing apparently randomly crystallized material. We believe this randomly crystallized material represents a second phase, which was still molten at the time the LaB_6 zone solidified, and which crystallized later when the zone cooled to a somewhat lower temperature. The melting point of LaB_6 is 2715° C [18].

The presence of rounded corners on the surface features of the second type is somewhat curious, giving these pits an almost artificial appearance. The rounded corners and smooth sides of the features are apparently related to the local phase equilibrium between solid LaB_6 and molten second-phase material during cooling.

Auger electron spectroscopic (AES) analysis of the material within the second type of feature can be summarized as follows. Scanning Auger microscope (SAM) maps (Fig. 4) of the region in and around a pit show carbon and oxygen enrichment and boron depletion inside compared with the smooth surrounding surface. Lanthanum also appears slightly depleted, but this is probably caused by reduced Auger electron detection sensitivity due to the geometry of the pit.

Careful AES point analyses are summarized in Table V, with typical spectra inside and outside the pit

TABLE V AES data for cleaved surface inclusion (pit) Ar^+ sputtered ~50 nm

Analysis point*	Peak-to-peak heights					Peak ratios			
	La(78)†	La(625)	B(179)	C(272)	O(510)	La(78)/ La(625)	B(179)/ La(625)	C(272)/ La(625)	O(510)/ La(625)
1	4.5	5.1	2.6	12.4	17.4	0.88	0.51	2.43	3.41
2	7.9	7.7	15.5	2.2	7.5	1.03	2.01	0.29	0.97
3	4.8	4.45	3.6	5.5	17.4	1.08	0.81	1.24	3.91
4	5.5	5.25	4.85	5.9	17.4	1.05	0.92	1.12	3.31
5	4.7	4.5	4.7	7.2	17.4	1.04	1.04	1.60	3.87
6	3.9	4.45	2.7	12.2	17.4	0.88	0.61	2.74	3.91

*Point 2 is on smooth surface outside pit. Other points inside pit (see Fig. 4a).
†Auger peak identification: La(78) = La(NOO) transition; La(625) = La(MNN); B(179) = B(KLL); C(272) = C(KLL); O(510) = O(KLL)

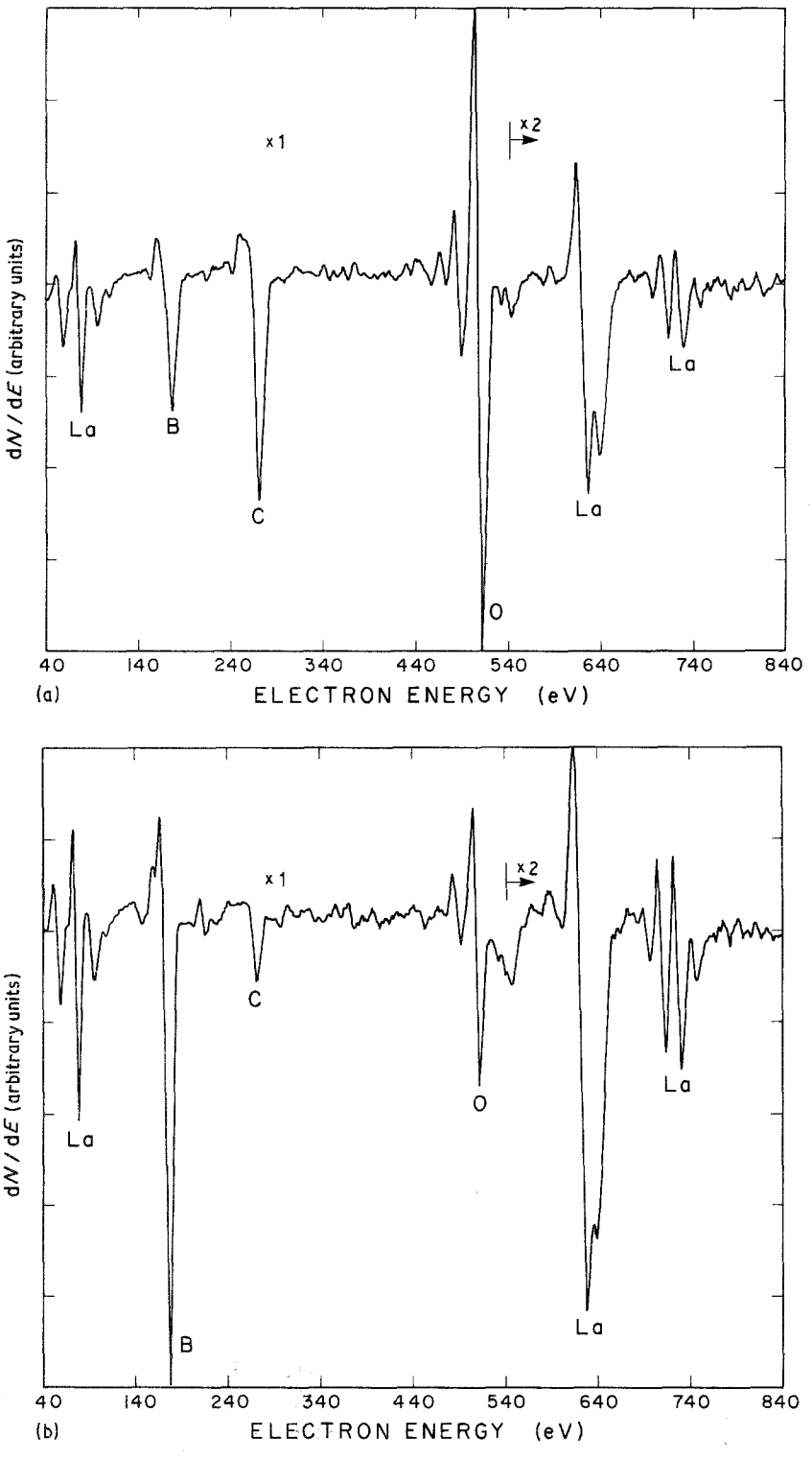

Figure 5 (a) Typical Auger spectrum of second-phase inclusion in pit, after sputtering 50 nm (Point 5); (b) Auger spectrum of smooth LaB_6 fracture surface, after sputtering 50 nm (Point 2).

shown in Figs. 5a and b, respectively, after sputter removal of approximately 50 nm of material. The La(78)/La(625) peak ratio is approximately the same inside and outside the surface feature, implying that the ratio of bulk to surface lanthanum concentrations is the same in both regions. However, the B/La(625) ratio in the second-phase material is $\sim 1/4$ to 1/2 times that in the surrounding LaB_6 surface. The O/La(625) ratio, on the other hand, is 3.5 to 4.0 times larger in the second phase than in the surrounding chemisorbed CO layer. Additionally, the La(625) peak (Fig. 5a) shows significant splitting in the second phase compared with the La(625) peak of LaB_6 (Fig. 5b). We have observed such splitting in previous studies of oxygen chemisorption on heated LaB_6 surfaces, where boron–oxygen and lanthanum–oxygen compounds are formed [28]. This splitting is *not* observed during CO chemisorption.

Taken together, these results strongly suggest that the second phase is an La–B–O ternary compound with stoichiometry in the range of $LaBO_2$ to LaB_2O_4, based upon the relative AES signals of boron and lanthanum in LaB_6 and oxygen in an adsorbed CO layer. The presence of a significant amount of carbon might suggest that it is also part of the compound. However, the fact that the carbon concentration varies by a factor of ~ 2.5 from point to point within the inclusion may indicate that a large part of the carbon was in solution in the molten second phase, precipitating as the second phase cooled and

TABLE VI Bulk properties of LaB_6 and $LaBO_3$

Material	Molecular weight ($g\,mol^{-1}$)	Theoretical density ($g\,cm^{-3}$)	Crystal structure
LaB_6	203.7	4.71	Cubic
$LaBO_3$	197.7	5.31	Orthorhombic (aragonite)

crystallized yielding an anisotropic distribution of carbon as observed.

We speculate that the second-phase material is the ternary compound $LaBO_3$. This compound has excellent thermal stability and should be formed under the preparation conditions of our specimens if oxygen is available. Our arc zone-refining step is performed in very low oxygen partial pressure ($< 10^{-5}$ torr) in an atmosphere of high-purity argon, so that oxidation may be minimized. However, oxygen is present in the hot-pressed starting material which we use, as already discussed.

Using the LaB_6 and $LaBO_3$ bulk properties shown in Table VI and assuming that all the bulk oxygen (240 p.p.m.) is combined as $LaBO_3$, we calculate a bulk fraction of 0.1 wt % (0.1 mol %) or 0.09 vol % of second-phase material in our zone-refined samples. This assumption represents the maximum amount of second-phase material possible, since during cooling of LaB_6 from the melt an equilibrium is established between the melt and the solid. Thus, some dissolved oxygen is expected in the solidified LaB_6, which would reduce the amount of second-phase material below 0.09 vol %. Furthermore, the precipitated $LaBO_3$ might itself contain dissolved oxygen, further reducing the volume of precipitate.

If we further assume that all observed large defects with included material in the cleaved surfaces in fact contain $LaBO_3$ precipitates, and that the concentration of these features is uniform throughout the bulk, then we arrive at an actual bulk concentration of 0.02 wt % of the second-phase material, in fair agreement with the value calculated above from the bulk oxygen concentration.

It is clearly undesirable to have inclusions of second-phase material in LaB_6 cathodes, since they contribute to surface non-uniformity and may affect electron emission spatial distributions. Thus, careful control of oxygen contamination in the hot-pressed starting material appears important. As can be seen from Table II, the level of oxygen present in commercially available hot-pressed RB_6 materials may be quite high. It is clear that the allowable oxygen concentration in the hot-pressed material is a parameter which must be minimized in order to minimize its effect on the resultant single-crystal material.

6.2. Defects induced by contamination of hot LaB_6 surfaces

A different sort of impurity problem was observed during long-term (several hundred hours) heating of LaB_6 cathodes, primarily due to contamination of the cathode surface from outside sources. The RB_6 materials are very reactive with most refractory elements and compounds except carbon, rhenium and TaC. Extensive studies of the effects and the likelihood of contamination have been performed. We find that almost any refractory material deposited or vaporized on to a clean LaB_6 surface causes localized disruption of the surface (Fig. 6). Table VII summarizes the effects of various contaminant materials that we have observed on LaB_6 surfaces subjected to long-term heating. We have not observed any surface inclusions in life-tested cathodes other than those incorporating metallic impurities. None of the second-phase La–B–O compound has been positively identified in the life-tested cathodes, even in cases where it was detected before heating. Apparently this material has higher volatility than LaB_6, and rapidly evaporates from heated surfaces.

It should be noted that in several cases submicrometre particles, more or less uniformly distributed, were observed in SEM studies of life-tested cathode surfaces, but energy dispersive X-ray analysis performed in the SEM is not very reliable on such small particles, and does not allow elements (boron, carbon or oxygen) to be detected. Furthermore, particles this small cannot be characterized in the scanning Auger microscope available to us. We therefore are uncertain of the composition of these particles. However, in

TABLE VII Effects of refractory contaminants on LaB_6 surfaces

Contaminant	Source of contaminant	Effect on surface
Mo	Vaporization from molybdenum cup initially used to hold sample	Micrometre and submicrometre sized particles protruding from surface (apparently forms Mo–La–B compound)
Re	Vaporization from rhenium cup used to hold sample	Micrometre and submicrometre sized particles protruding from surface (apparently forms Re–La–B compound)
TaC	Dusted on to surface during mounting procedure, not properly cleaned	Pits form around TaC particles (local faceting to radius of about five particle diameters)
Mg, Si, O	Probably bulk contaminant not removed during zone refining	Particles several μm in diameter

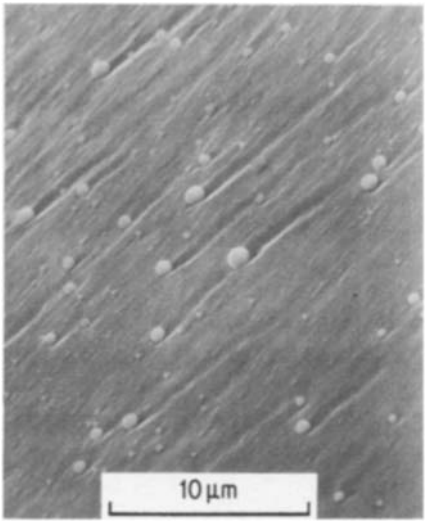

Figure 6 SEM photo of surface features produced by rhenium evaporation on to a clean LaB_6 surface.

every case where the small particles were observed, larger particles containing metallic impurities were also seen, so we assume the smaller particles to be of similar composition.

The consequences for the emission properties of having contaminant particles present in the cathode surfaces do not seem to be particularly severe as long as the total coverage is not large. Individual particles may cause local increases in volatility and changes in stoichiometry and morphology of the surface, possibly reducing emission from the affected area and reducing overall cathode lifetime. The emission distribution may also be disturbed by the presence of contaminant particles. None of these effects has been investigated quantitatively. Our approach has been to avoid the contamination and thus remove any associated difficulties.

7. Conclusions

Reproducible means of producing and characterizing oriented single crystals of LaB_6, CeB_6 and PrB_6, in the range of 1 to 3 mm diameter, have been developed. An overall decrease in the B/La ratio of LaB_6 with increasing number of zone passes was observed and was attributed to preferential volatilization of boron from the melt. In addition, a positive gradient in the B/La ratio in the zone pass direction along the specimen was observed for a feedstock composition of B/La < 6.2, in accord with accepted zone-refining theory and the reported LaB_6 phase diagram. Cathode pellets cut from these crystals have been mounted in rugged structures and have demonstrated long operational lifetimes.

A comparison of the bulk purity of arc float-zone and laser float-zone refined LaB_6 materials has been made, based on the current work and data available in the literature. The arc zone-refining technique appears to be superior to the laser zone-refining method in removing metallic impurities from the starting material, although the reason for this is not clear.

An investigation of the defects presented in zone-refined LaB_6 specimens suggests that O_2 contamination in the starting material may be a critical factor. This O_2 combines with lanthanum, boron and possibly carbon, producing second-phase precipitates during cooling of the melt which are observable in cleaved specimens. Subsequent heating removes this second-phase material from cleaved surfaces, indicating a volatility greater than that of LaB_6 itself. O_2 contamination in the starting materials should be minimized in order to maintain uniform surface topography.

The effects of external contamination of single-crystal LaB_6 surfaces with refractory materials such as molybdenum, rhenium and TaC have also been studied. These materials coalesce into various sized particles, generally forming compounds with lanthanum and boron and causing local surface disruption which is undesirable where cathode uniformity is critical. Cathode mounting structure assembly procedures should be designed to remove excess powdered braze material from the cathode surface, and to prevent a line-of-sight arrangement between the cathode surface and heated support elements.

Acknowledgements

This work was supported by RADC/Solid State Sciences Division, Hanscom AFB, under Contract No. F19628–80–C–0117 and by the Air Force Office of Scientific Research, USAF, under Grant No. AFOSR 83–0105. The US Government is authorized to reproduce and distribute reprints for Governmental purposes notwithstanding any copyright notation thereon.

References

1. L. W. SWANSON, M. A. GESLEY and P. R. DAVIS, *Surf. Sci.* **107** (1981) 263.
2. E. STORMS and B. MUELLER, *J. Phys. Chem.* **82** (1978) 51.
3. *Idem, J. Appl. Phys.* **50** (1979) 3691.
4. T. AITA, U. KAWABE and Y. HONDA, *Jpn. J. Appl. Phys.* **13** (1974) 391.
5. M. FUTAMOTO, T. AITA and U. KAWABE, *ibid.* **14** (1975) 1263.
6. I. ZUBECK, R. FEIGELSON, R. HUGGINS and P. PETITT, *J. Cryst. Growth* **34** (1976) 85.
7. T. TANAKA, E. BANNAI, S. KAWAI and T. YAMANE, *ibid.* **30** (1975) 193.
8. T. TANAKA, R. NISHITANI, C. OSHIMA, E. BANNAI and S. KAWAI, *J. Appl. Phys.* **51** (1980) 3877.
9. E. E. WINDSOR, *Proc. IEE* **116** (1969) 348.
10. T. TAKAGI and M. ISHII, *J. Cryst. Growth* **40** (1977) 1.
11. F. J. HOHN, T. H. P. CHANG, A. N. BROERS, G. S. FRANKEL, E. T. PETERS and D. W. LEE, *J. Appl. Phys.* **53** (1982) 1283.
12. J. S. HAGGERTY, presented at American Association Crystal Growth New England Section Meeting, October 1979 (unpublished).
13. P. HAFNER and E. B. BAS, in Proceedings of 7th International Conference on Electron and Ion Beam Science and Technology, Washington, DC, May 1976, edited by R. Bakish (Electrochemical Society, Princeton, New Jersey, 1976).
14. E. B. BAS, P. HAFNER, A. A. LATIF and G. WULFF, in Record of 11th Sympsium of Electron, Ion and Laser Beam Technology, San Francisco, May 1971, edited by R. F. M. Thornley (San Francisco Press, 1971).
15. J. VERHOEVEN, E. D. GIBSON, M. A. NOACK and R. J. CONZEMIUS, *J. Cryst. Growth* **36** (1976) 115.
16. S. MOTOJIMA, Y. TAKAHASHI and K. SUGIYAMA, *ibid.* **44** (1978) 106.
17. E. I. GIVARGIZOV and L. N. OBOLENSKAYA, *ibid.* **51** (1981) 190.

18. O. A. MORDOVIN and E. N. TIMOFEEVA, *Russ. J. Inorg. Chem.* **13** (1968) 1627.
19. V. I. ALEKSANDROV, V. V. OSIKO, A. M. PROKHOROV and V. M. TATARINTSEV, *Vestnik Akademii Nauk SSSR* (1973, No. 12) 29.
20. S. F. VOGEL, *Rev. Sci. Inst.* **41** (1970) 585.
21. I. M. KOLTHOFF and P. J. ELVING (eds), "Treatise on Analytical Chemistry, Part II", Vol. 20 (Wiley, New York, 1978) p. 55.
22. J. W. TERESHKO, *Anal. Chem.* **35** (1963) 157.
23. C. N. REILLEG, R. W. SCHMID and D. W. LAMSON, *ibid.* **30** (1958) 953.
24. G. SCHWARZENBACH and H. FLASHKA, "Complexometric Titrations", translated by H. M. N. H. Irving (Methuen, London, 1969) p. 194.
25. J. S. FRIK, R. T. OLIVER and D. J. PIETRZYK, *Anal. Chem.* **30** (1958) 1111.
26. W. G. PFANN, "Zone Melting", 2nd edn (Krieger, Huntingdon, New York, 1978) p. 27.
27. M. A. NOACK and J. D. VERHOEVEN, *J. Cryst. Growth* **49** (1980) 595.
28. P. R. DAVIS and S. A. CHAMBERS, *Appl. Surf. Sci.* **8** (1981) 197.

Received 25 March
and accepted 23 April 1985